International Journal of
Turbomachinery
Propulsion and Power

MDPI

Article

An Experimental and Numerical Investigation into Compressor Casing Heat Shield Effectiveness †

Andrew Pilkington [1,*], Vinod Gopalkrishna [2], Christopher Barnes [2], Leo Lewis [1] and Marko Bacic [1,2]

[1] Oxford Thermofluids Institute, University of Oxford, Oxford OX2 0ES, UK; marko.bacic@rolls-royce.com (M.B.)
[2] Rolls-Royce PLC., Derby DE24 8BJ, UK
* Correspondence: andrew.pilkington@eng.ox.ac.uk
† This manuscript is an extended version of the ETC16-164 meeting paper published in the Proceedings of the 16th European Turbomachinery Conference, Hannover, Germany, 24–28 March 2025.

Abstract

An investigation was conducted into the effectiveness of heat shields in an aero-engine compressor casing to slow down thermal time constants. The investigation used a combination of experimental measurements from a full-size compressor casing rig, combined with numerical analysis using CFD and thermal modelling. Experiments were performed on a compressor casing both with and without heat shielding in order to determine the heat shield effectiveness. Temperature measurements were taken throughout the casing in order to determine the thermal time constants. The experimental data was then used to validate a thermal model and CFD simulations of the compressor casing. The modelling allowed the heat transfer coefficients in the compressor casing to be determined from the experimentally measured time constants. It was found that the heat shields gave an increase in thermal time constant at each measured location. With a doubling in the time constant at some locations compared to the unshielded case. It was also found that the heat shields need to be fully sealed, as leakage flows significantly reduce their effectiveness.

Keywords: heat shield; heat transfer coefficient; compressor casing; thermal time constant

1. Introduction

The compressor casing in an aero-engine is heated by hot bleed air from the compressor offtake. The convective heating from the offtake air causes thermal expansion of the compressor casing, typically at a faster rate than the compressor discs holding the blades. The faster rate of thermal growth of the casing relative to the discs causes an increase in tip clearance of the compressor blades. This increased clearance is undesirable as it results in reduced efficiency and operability of the compressor [1,2]. In order to slow down the thermal expansion rate of the casing and increase the casing thermal time constant, heat shields can be used. The heat shields stop the bleed air from impinging on the casing and have the effect of reducing the heat transfer coefficient (HTC). The downsides of adding heat shields are the increased cost, weight and complexity of engine assembly, so the performance benefit must outweigh these downsides. The aim of this investigation was to quantify the increase in thermal time constant and HTC reduction from the use of heat shields.

There is very little data in the literature about the heat transfer in a compressor casing and how this can be affected by the use of heat shields. A numerical investigation was conducted by Malavade et al. [3] where several methods to increase the time constant of

Academic Editor: Antoine Dazin

Received: 7 June 2025
Revised: 15 July 2025
Accepted: 21 July 2025
Published: 2 February 2026

a compressor casing were analysed. It was found that adding heat shields was the most effective method, over methods such as adding fins or a thermal barrier coating to the casing, or increasing the casing thickness. The main focus of Malavade et al., however, was on the mechanical design of the heat shield. A similar investigation by Riahi and Borns [4] was conducted on the mechanical design of a combustor heat shield, where the HTC were provided by flat plate and channel flow correlations.

Measuring the effectiveness of a heat shield in a full aero-engine test is difficult, with the cost of a back-to-back test, with and without heat shields, being prohibitively high. Also, different builds of an engine often feature many changes, making it difficult to isolate the true effect of the heat shields.

This investigation [5] builds on previous work by Pilkington et al. [6] where the Transient Heat Transfer Facility (THTF) at the Osney Thermofluids Institute was shown to be able to measure thermal time constants in a full-size compressor casing. The use of this facility allows for true back-to-back testing in an engine realistic environment, and the results can therefore demonstrate technology readiness level 6 (TRL6). To the author's knowledge, this is the first investigation where back-to-back heat transfer experiments on a full-size compressor casing have been conducted.

2. Experimental Investigation

2.1. Test Facility

The Oxford Transient Heat Transfer facility (THTF) used in this investigation is shown in Figure 1. The facility comprises a 2 m diameter spherical pressure vessel, connected to a heated high-pressure air supply. The pressure vessel is large enough to accommodate full-sized components from a large civil aero-engine and can be tested at engine representative conditions. The development and initial application of the facility are described by van Paridon et al. [7] and Dann et al. [8].

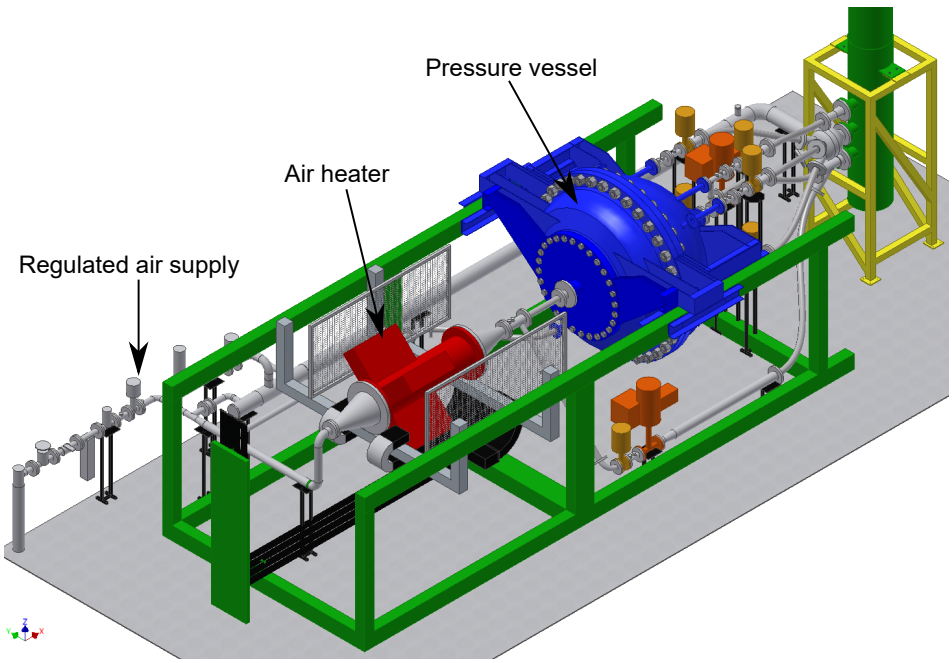

Figure 1. Transient heat transfer facility overview.

Compressed air for the rig is sourced from a tank, initially at 28 bara, which is regulated down to the experimental test pressure of 12 bara. The setup can maintain a flow of 2.4 kg/s for around 8 min. The air is heated by an Osram 600 kW electric heater up to a set temperature of 200 °C, before entering the facility and the experimental test section, as

shown in Figure 2. The air exits the pressure vessel through four pipes, each containing a choked orifice and controlled by a separate valve, allowing the rig mass flow rate to be controlled.

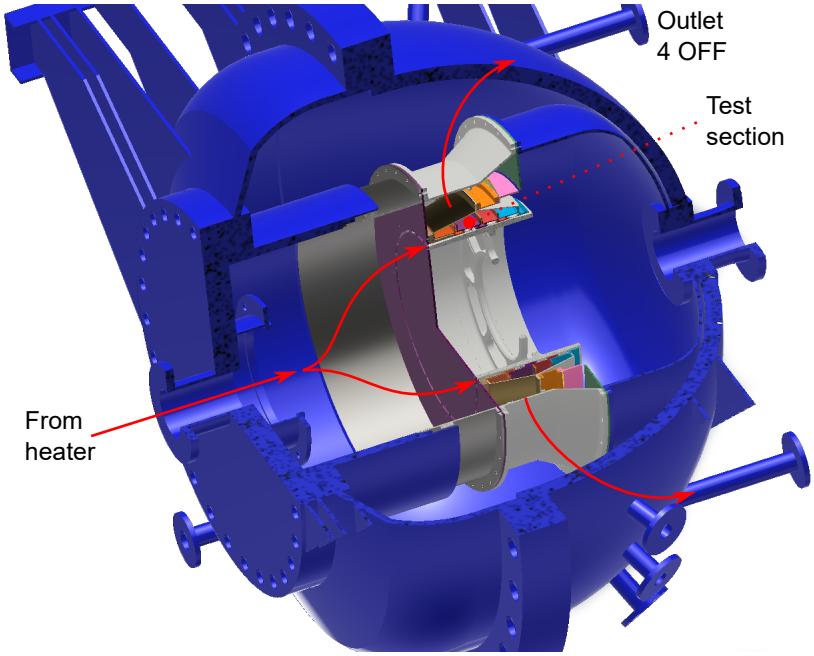

Figure 2. Cutaway of pressure vessel containing test section.

The test section inside of the pressure vessel is shown in Figure 3. The test section was constructed from a high-pressure compressor (HPC) inner casing from a current large aero-engine, which consists of the rearmost four stages of the compressor. Included in the inner casing are several bolted flanges; the heat transfer on these flanges is a significant factor in the thermal response of the casing. The heat shields are designed to cover these flanges and reduce the flange HTC.

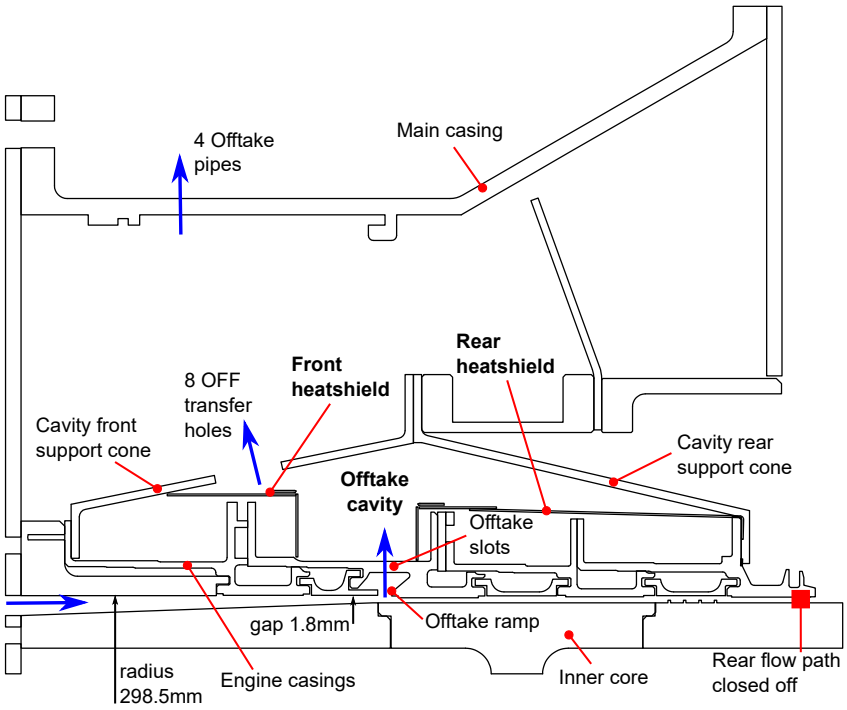

Figure 3. Cross-section schematic of test section.

The test section was first investigated without the heat shields fitted to establish a baseline thermal response. The experiments were repeated after the test section was stripped and rebuilt with the heat shields fitted. The heat shields were constructed from 0.7 mm thick SAE 304 stainless steel, rolled into shape and bolted to the casing. Small gaps were sealed with 'Silcoset 152' sealant where access was possible. The rear heat shield can be seen in Figure 4.

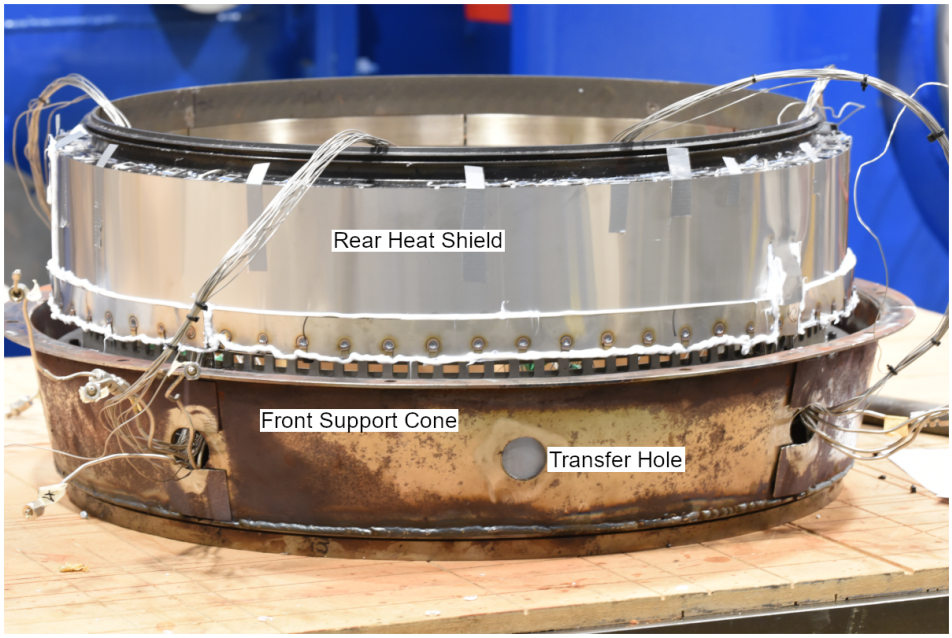

Figure 4. Test section partially assembled showing rear heat shield.

The air enters the test section through an annular slot, which was created by adding a cylindrical inner core inside of the casing, giving a nominal 1.8 mm radial gap and an annulus outer radius of 289.5 mm. Outboard of the casing are front and rear support cones, which form a cavity for offtake air. The air enters the offtake cavity through annular offtake slots and exits through eight equi-spaced 32 mm diameter transfer holes in the cavity front support cone. The air exits the test section through four exit pipes connected to the pressure vessel outlets.

It is the airflow in this offtake cavity that determines the convective HTC on the casing and the flanges. The aim of the heat shields is to modify the flowfield in this region, providing a low velocity region around the casing flanges and directing the bulk of the air from the offtake slot to the transfer holes.

This arrangement of a flanged compressor casing supported by conical sections, an offtake slot, and air transfer holes, is representative of the arrangement found on a large civil aero-engine.

2.2. Instrumentation

Thermocouples were used to measure the thermal response of the metal casing to a change in driving air temperature. The thermocouple locations are shown in Figure 5, where metal temperature thermocouples have been labelled as locations 1 to 12 and air thermocouples labelled as A2 to A4. Not shown in Figure 5 is location A1, the heater exit air temperature. Metal thermocouples at locations 1, 7 and 8 were underneath the front heat shield, locations 3–6 and 9–11 were under the rear heat shield and locations 2 and 12 were not covered by a heat shield. Four thermocouples were mounted at each location, spaced circumferentially 90° apart, in order to measure any circumferential non-uniformity of the temperature field.

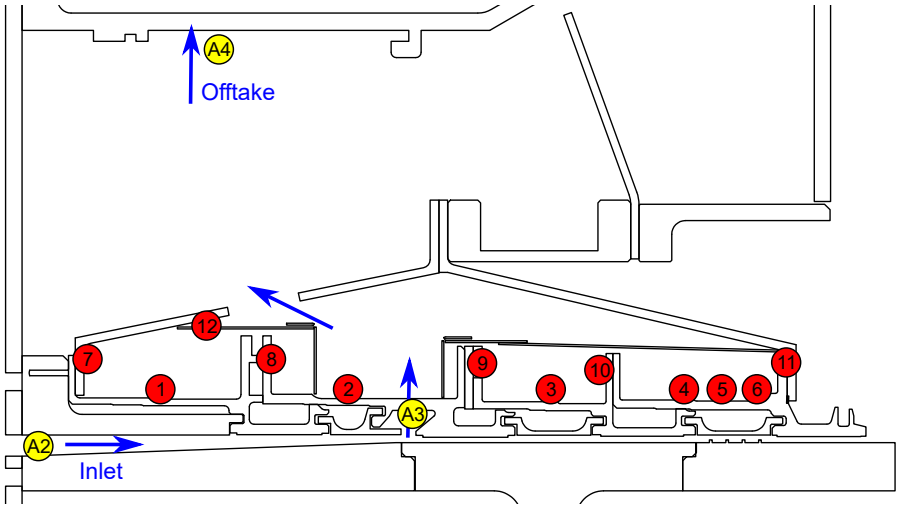

Figure 5. Air and metal thermocouple locations in test section.

The thermocouples were all 1 mm diameter, mineral-insulated and type K, with an accuracy of ±2.5 °C. The thermocouple data was recorded at a rate of 10 Hz. It was found that the air thermocouple time constant was 6 s; this delay was corrected out in the analysis of the response rate of the casing metal thermocouples.

2.3. Test Conditions

One of the aims of this investigation was to test under realistic engine conditions to avoid the need to scale the results. The experiment used a real engine compressor casing; therefore, no geometric scaling was required. The testing was also conducted using the full scale offtake mass flow rate, therefore giving an engine representative offtake Reynolds number.

The nominal mass flow rate through the test section and offtake was 2.4 kg/s in order to match engine conditions, see Table 1. Experiments were also conducted at 1.2 kg/s to provide further datasets for validation of the thermal model. The lower mass flow runs only opened two of the four outlet valves; otherwise, the experimental procedure was the same.

The air entering the test section was heated using an electric heater, which allowed for a fast ramp in inlet air temperature from ambient up to 200 °C. The response of the metal thermocouples to this change in air temperature was used to determine the thermal response at the different locations. Only one test was performed a day; this gave the facility time to cool overnight to a uniform starting temperature.

Table 1. Summary of nominal test conditions.

Mass Flow	2.4 kg/s
Temperature	200 °C
Pressure	12 bara
Casing diameter	597 mm
Offtake Reynolds No.	8.1×10^{6}

2.4. Experimental Results

The temperature response at each location was recorded for runs both with and without heat shields fitted; an example of the response is shown in Figure 6. The responses are characterised to produce thermal time constants, which show how quickly the casing responds to a change in driving air temperature. Full details of the characterisation method

are given in [6], but the method is based on a lumped mass approach and accounts for the finite heat capacity of the driving air.

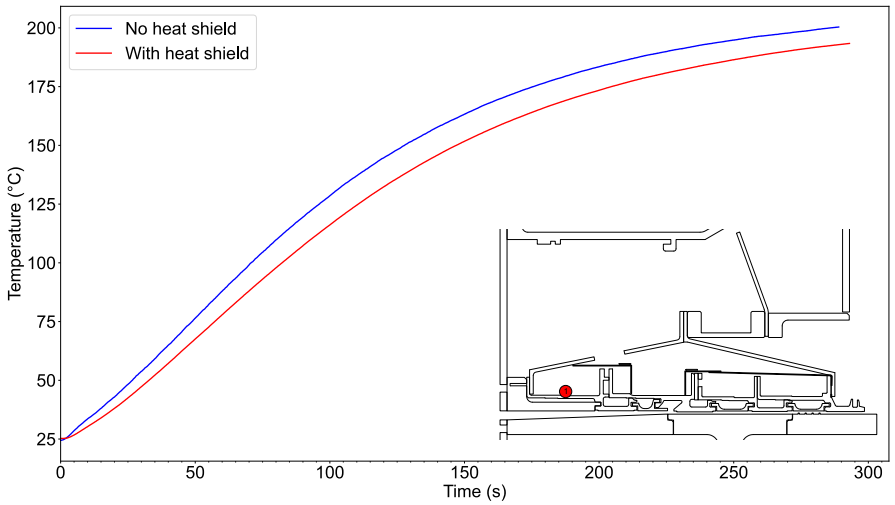

Figure 6. Metal temperature response at location 1, without and with heat shields fitted.

$$T_M = T_0 + (T_{in} - T_0)(1 - e^{-ta/b}) \tag{1}$$

This metal temperature responds with a single time constant $\tau = b/a$. Where b is the intrinsic time constant of the block and a is the source strength, which accounts for a driving fluid with finite heat capacity.

$$a = \frac{1}{1 + \frac{hA}{\dot{m}c_p}} \tag{2}$$

$$b = \frac{MC}{hA} \tag{3}$$

The characterisation was performed at each location for the experiments with and without the heat shields fitted, with the data plotted in Figure 7.

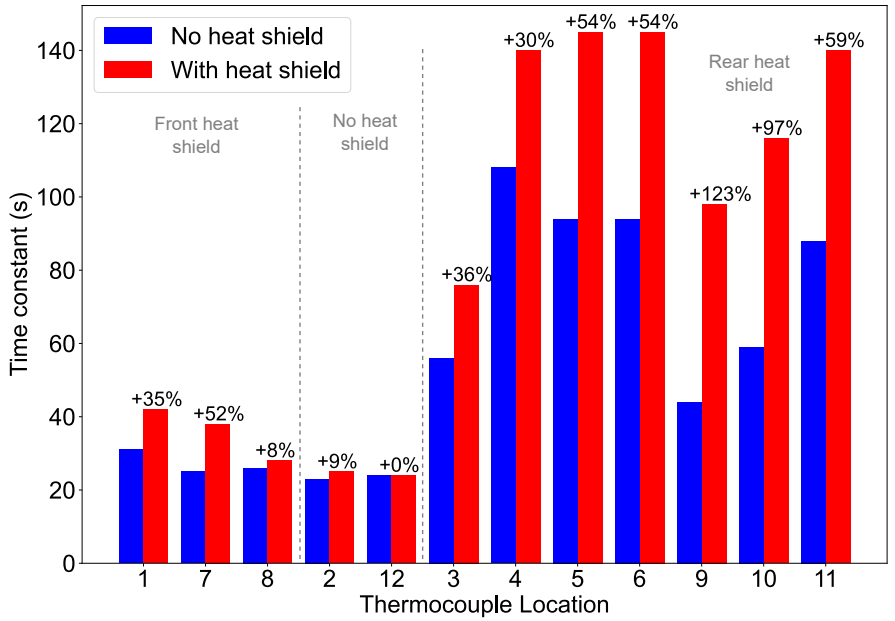

Figure 7. Metal thermal time constants, without and with heat shields fitted.

It can be seen that the heat shields have performed well, giving an increase in casing time constant at each location they covered. The locations not covered by the heat shields, 2 and 12, showed small or no changes to the time constant. In particular, the rear heat shield can be seen to be very effective, with the time constant increasing in the range of +30% to +123%. The front heat shield was found to give a smaller increase in casing response time, ranging from +8% to +52%. This is likely due to imperfect sealing of the heat shield in this location, allowing a leakage flow behind the heat shield. The rig geometry is comparable to a real engine, so the area around the heat shields is difficult to access during assembly and to ensure perfect sealing.

The time constants were determined by taking a circumferential average of the thermocouple readings at each location. However, it was found there was no notable circumferential variation in the readings, with variations between thermocouples within the measurement accuracy. This result shows the heat transfer in the cavity is dominated by forced convective heat transfer, with buoyancy effects being negligible.

A secondary measure showing the effectiveness of the heat shields is to perform an enthalpy balance of the air entering and exiting the test section. The enthalpy change in the air is calculated from the measured mass flow rate and the air thermocouples at locations A2 and A4, at the test section inlet and outlet, respectively.

The enthalpy reduction in the air from the inlet to the outlet is shown over the duration of the heating phase of a test in Figure 8. It can be seen that after the heat shields were fitted, the enthalpy reduction was lower, showing the air had lost less heat to the compressor casing. Throughout most of the run, the heat shield case showed a 10% lower enthalpy reduction compared to the no heat shield case. As the 10% was a global change across the whole test section, the heat shields would have to be locally more effective than this at reducing heat transfer.

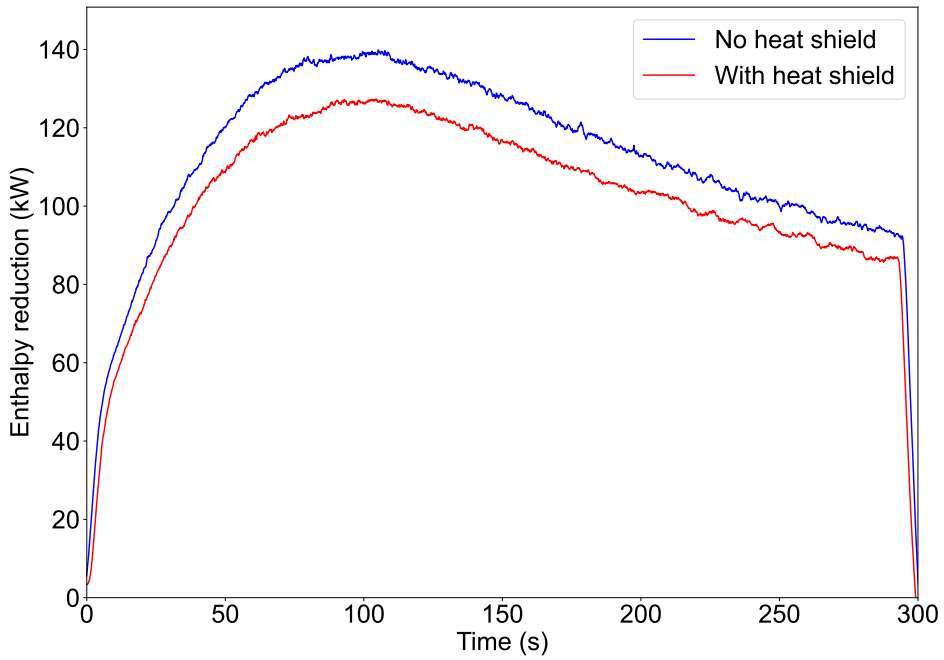

Figure 8. Enthalpy reduction in air from inlet to outlet, without and with heat shields fitted.

Therefore, the experimental results show that the heat shields are effective in reducing the thermal time constants of the casing.

3. Numerical Investigation

3.1. Method

Numerical investigation of the experimental results was carried out using ANSYS SpaceClaim and Fluent packaged in version 19.1 for the CFD and Roll-Royce Plc's in-house proprietary finite element solver called SC03. The overall approach of the numerical investigation consisted of 6 main steps:

1. Use ANSYS SpaceClaim to simplify the CAD geometry used in the experiment, making it water-tight, extracting fluid volume and preparing it for meshing.
2. Use ANSYS Fluent to generate the CFD mesh with multiple layers of prismatic cells at the wall boundaries, ensuring appropriate mesh resolution to capture the heat transfer behaviour and filling the remaining volume with poly-hexa cells.
3. Apply boundary conditions and converge the CFD model—first steady state and unsteady if required.
4. Identify dominant flow structures by post-processing the CFD results. Extracting data from the CFD model to define boundary condition positions, mass flow splits, recirculations and heat transfer coefficients in SC03.
5. Create the SC03 model and run through the transient cycle.
6. Compare the SC03 model results to the test data. Make physically justifiable modifications to the model if necessary, to match the numerical results to measurements.

3.2. CFD Setup

The CFD geometry for both the cases, with and without the heat shields in the offtake cavity, consisted of a 90° sector, including the annulus, 25 offtake slots, an offtake cavity, 2 offtake flow transfer holes, the offtake flow collection chamber, and an offtake flow exit hose. The geometry for the two cases is shown in Figures 9 and 10. The offtake flow collection chamber is included in the CFD domain to eliminate any influence of the outlet boundary condition on the offtake cavity flow pattern. For the heat shielded case, a smaller collection chamber is created, Figure 10, to reduce the number of computational cells.

Since heat transfer data was required, the mesh needed to be of sufficiently high quality, especially near the walls, to capture boundary layer effects. To that end, several prism layers (typically around 17) were defined adjacent to the walls, with the remainder of the volume filled with poly-hexa cells. The near-wall spacing is set such that the y^+ values were typically 1 and always less than 5, especially on the walls from which heat transfer data was to be extracted. The surface and volume mesh of the non-heat shielded cavity is shown in Figure 9.

A mesh independence study was carried out with three different mesh densities, nearly doubling the cell count from coarse to nominal to fine meshes for the non-heat shielded case. The three meshes showed negligibly small variation in the pressure drop prediction from the inlet to outlet. The circumferentially averaged heat flux distribution, on the inner walls of the cavity, showed ∼0.5 % variation between coarse and fine mesh results. The fine mesh was used for the investigation; the final cell counts for the non-heat-shielded and heat-shielded cases were 32 million and 28 million, respectively.

Steady and unsteady simulations were carried out using 2nd order schemes for pressure, flow, turbulence and energy equations. Realizable k-ϵ (RKE) with enhanced wall treatment equations were used for turbulence modelling. The stabilized max temperature condition from the experiment run was chosen for the CFD simulation in both cases.

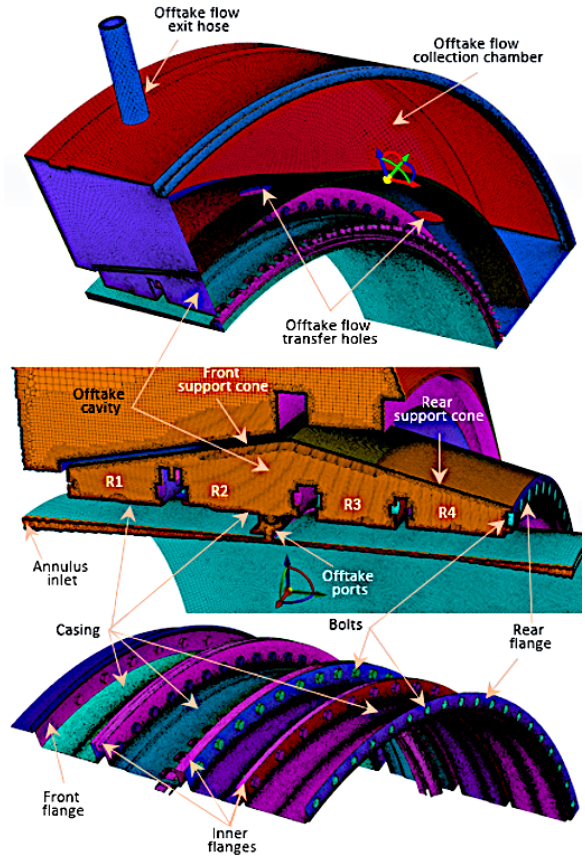

Figure 9. Surface and volume mesh of the cavity without heat shields.

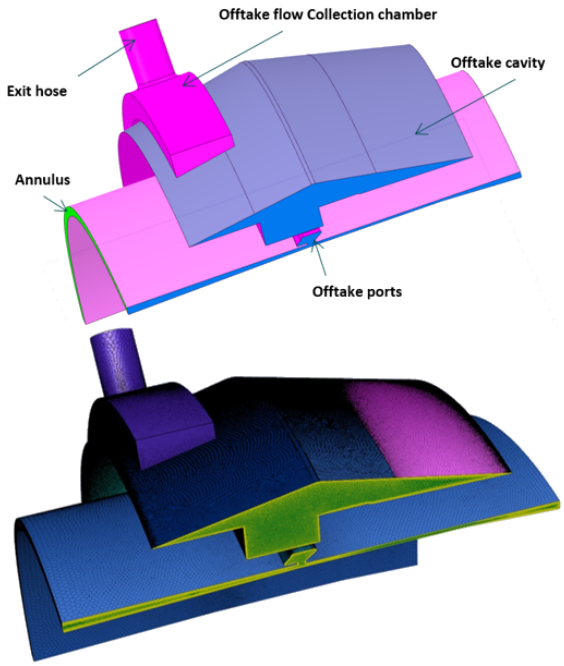

Figure 10. Geometry and mesh of the cavity with heat shields.

Ideal gas was used as the working fluid with a 'Mass Flow Inlet' type boundary condition at the annulus inlet. For the non-heat shielded case, a mass flow rate of 0.505 kg/s, total temperature of 480 K, turbulence intensity of 5% and hydraulic diameter of 3 mm with direction of flow normal to the boundary were used at the inlet. For the heat shielded case,

the inlet mass flow rate and temperatures were changed to 0.493 kg/s and 479 K. At the exit of the offtake hose, 'Pressure-outlet'-type boundary conditions with a back pressure of 9.5 bara, back flow temperature of 450 K, 5% turbulence intensity and 22 mm hydraulic diameter were used for both cases. Except the inner walls of the offtake cavity, all other walls were assumed to be adiabatic. On the cavity walls, constant temperature boundary conditions were applied, with the stabilized maximum metal temperatures being used. The pressure-based coupled solver, with a Courant Number of 80 and an under-relaxation factor of 0.6 for both pressure and momentum equations, was used for the CFD simulations. All other under-relaxation factors were set to 1.

Solution convergence for the non-heat shielded case was achieved after ~18,000 iterations, with continuity and velocity residuals reduced by an order of 3 and the energy, k and ϵ residuals by an order of 4. The mass flow and energy imbalance in the domain were less than 0.01% and 0.1%, respectively. When the simulations were continued by switching the solver to 2nd-order unsteady simulations, the residuals further dropped by two orders of magnitude, and very good convergence was obtained.

For the heat shielded case, very good convergence was achieved after ~15,000 iterations. Mass and energy imbalances were less than 0.05% for this case.

3.3. CFD Results

3.3.1. Non-Heat Shielded Cavity

If the cavity is grossly divided into four sub-regions (say R1 to R4, as shown in Figure 9) separated by the flanges, Figure 11 indicates that the velocities are significantly higher in the two front sub-regions (i.e., highest in R2, directly above the offtake ports, followed by R1) compared to the two rear sub-regions (R3 and R4).

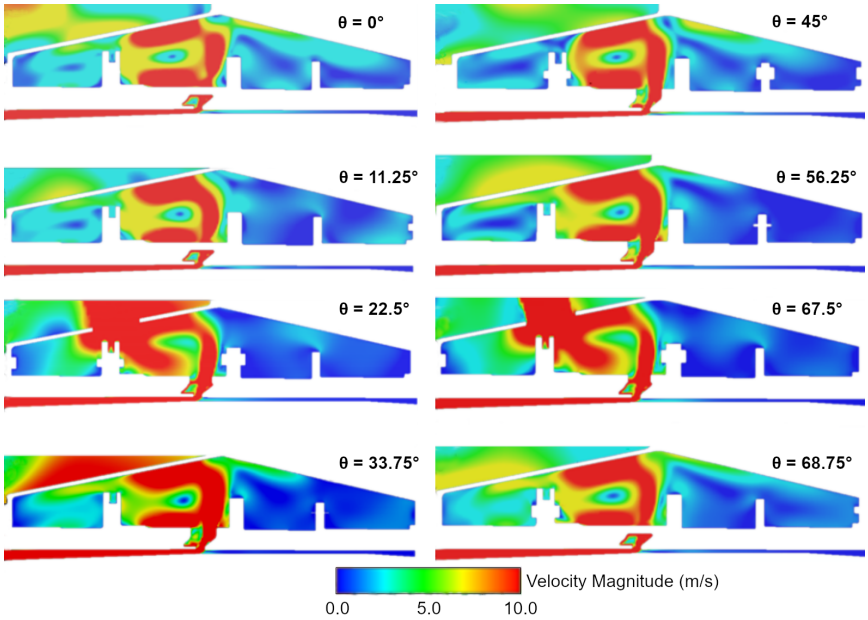

Figure 11. Velocity magnitude contours at eight iso-circumferential locations in the non-heat shielded cavity.

For the non-heat shielded cavity, the mean velocity magnitude contours are shown in Figures 11 and 12. These figures show a strong doughnut-shaped recirculation in R2, which remains mostly axisymmetric. This flowfield is caused by the jets from the offtake impinging on the roof of the front support cone and recirculating in the sub-region R2. Part of the flow, after impingement, flows all the way up to the front flange and recirculates in sub-region R1 before exiting the cavity.

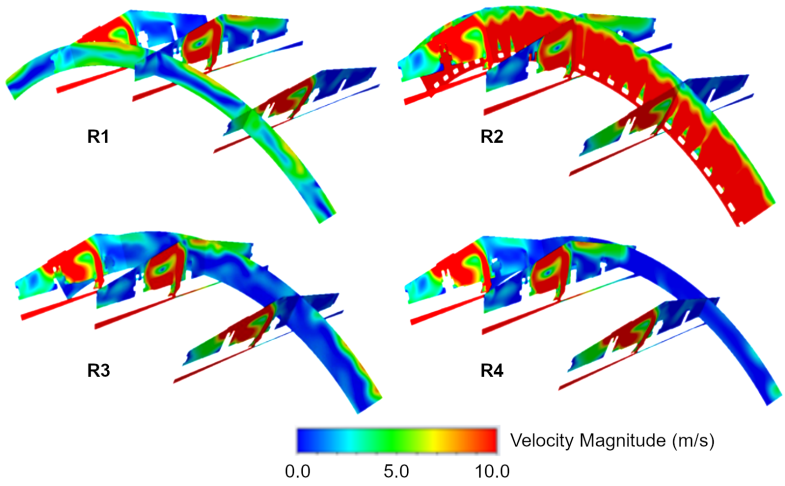

Figure 12. Velocity magnitude shown on four iso-axial planes, located approximately near the centre of sub-regions R1 to R4, in the non-heat shielded cavity.

Examination of the velocity vector plots at three iso-circumferential locations, Figure 13, shows that the recirculation in R1 can also be considered axisymmetric. In the other two sub-regions, R3 and R4, although the flow is non-axisymmetric, the velocities are an order smaller than those in R1 and R2. Hence, approximating the overall flow in the offtake cavity as axisymmetric should yield satisfactory results in the finite element modelling.

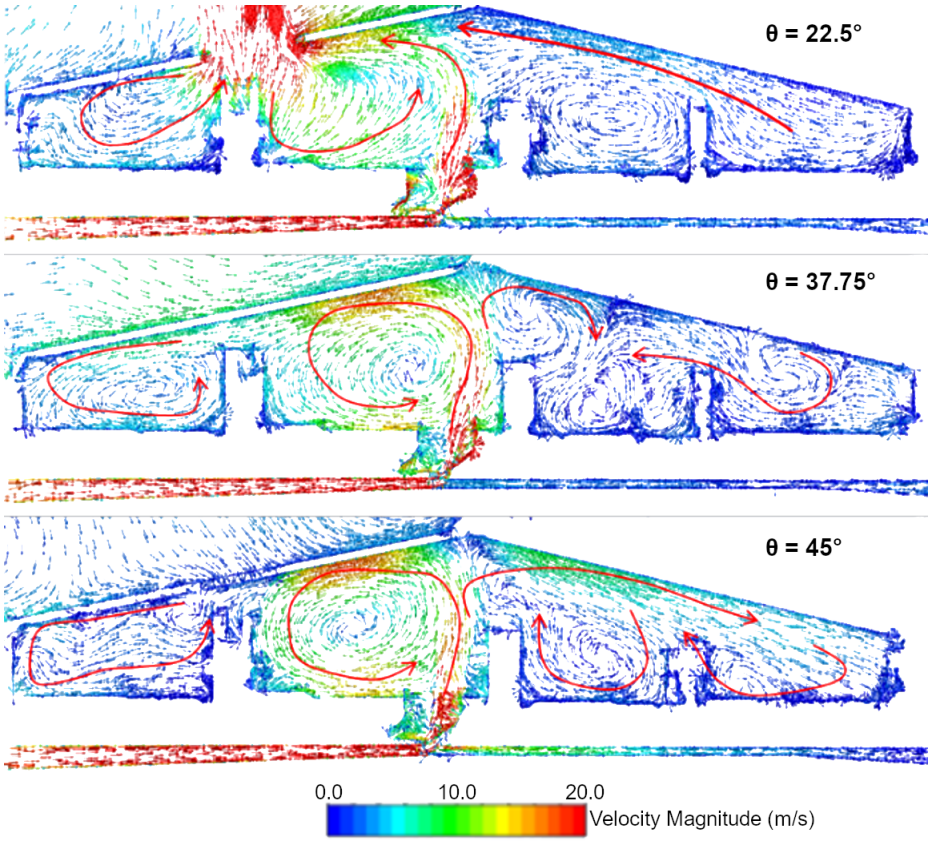

Figure 13. Constant length vector plots coloured by velocity magnitude, plotted on three iso-circumferential planes, in the non-heat shielded cavity.

3.3.2. Heat Shielded Cavity

For the heat shielded cavity, the contour plots of mean velocity magnitude on four equi-spaced, iso-circumferential surfaces are shown in Figure 14. CFD predicts a strong

counter-clockwise recirculation in sub-region R2, where the offtake flow enters the cavity, and a weak clockwise recirculation occurs in sub-region R3 above the rear heat shield.

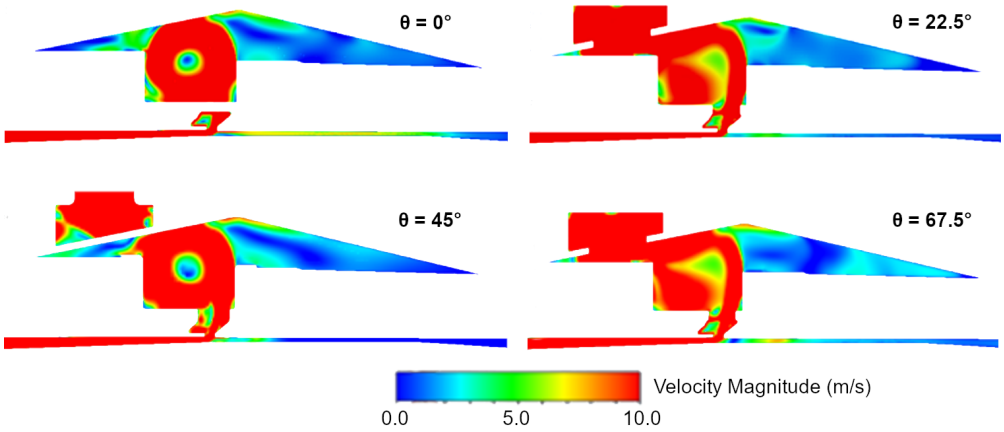

Figure 14. Velocity magnitude contours at four iso-circumferential locations in the heat-shielded cavity.

3.4. The 2D Flow Network Model

The finite element model (FEM) is 2D axisymmetric. To apply the boundary conditions in this model, a 2D flow network, closely resembling the 2D axisymmetric flow solution inside the offtake cavity, is created, shown in Figure 15. By clipping the iso-axial surfaces (shown in Figure 12) based on the axial flow direction, ±mass flows in the recirculating structures are calculated. Note that the leakage flows through stator cavities shown in the figure are not modelled but derived during the 'thermal matching' exercise explained in Section 3.6.

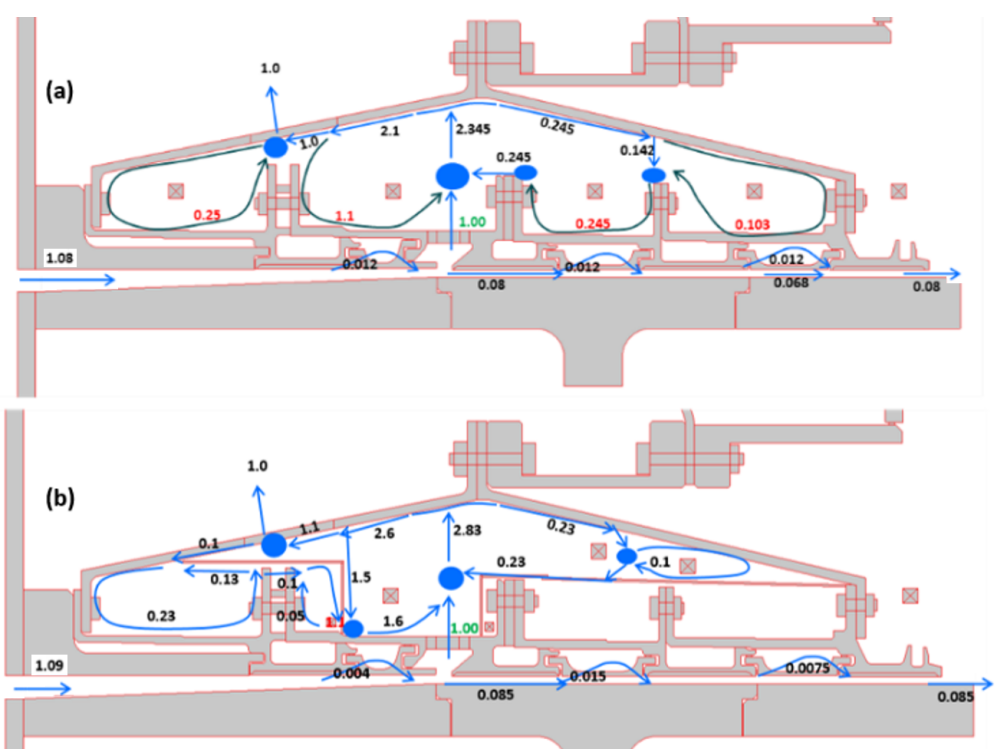

Figure 15. The 2D axisymmetric flow-network model approximately representing the flow inside the offtake cavity of the (**a**) non-heat-shielded case and (**b**) heat-shielded case. The numerical values are the non-dimensional mass flow rates in the recirculating flows non-dimensionalised using the off-take mass flow rate.

Further CFD simulations with reduced inlet flows, at 50% and 20% of the nominal, for the cases with and without heat shields, yielded similar flow patterns and non-dimensional flow networks.

3.5. Finite Element Modelling

Two-dimensional axisymmetric finite element thermal models of the rig were created for both cases using Rolls-Royce Plc's in-house FEM solver called SC03.

After assigning appropriate material properties to the solid domains in the FEM model, one-dimensional convective-type thermal boundary conditions (called "stream" boundary conditions) were applied on the solid/fluid interfaces to mimic the 2D flow network shown in Figure 15. The streams are interconnected to form the flow network, with mass and energy being conserved throughout.

The Nunner correlation [9], Equation (4), with mass flow rate, hydraulic diameter, and cross-sectional area of the recirculating flow as inputs, was used for heat transfer calculations in the streams. If the recirculation is approximated as an ellipse, as shown in Figure 16, then the area and hydraulic diameters are calculated assuming that the effective flow area on one side of the recirculation is equal to the area of an annular strip whose radial extent is 1/5th the outer radius of the minor axis of the ellipse (i.e., R in Figure 16).

$$Nu = \frac{\lambda PrRe}{8\left(1 + 1.5Pr^{-1/6}Re^{-1/8}\left(\frac{\lambda Pr}{\lambda_0} - 1\right)\right)} \tag{4}$$

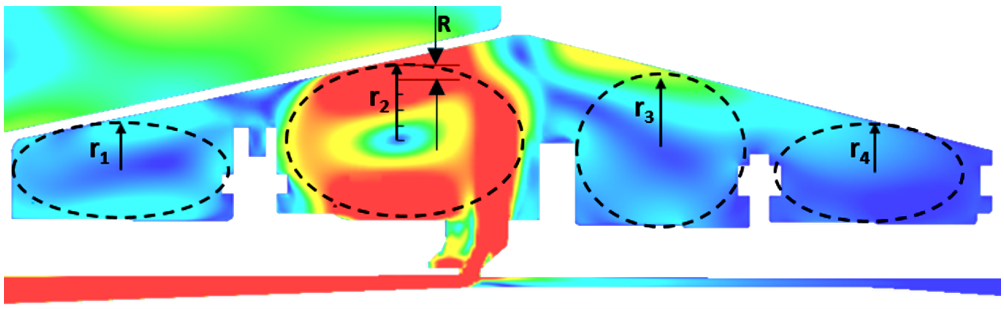

Figure 16. Illustration of length scale used for hydraulic diameter calculations in the Nunner Correlation for each sub-region.

3.6. Thermal Matching

The FEM model was run for the transient cycle, and the metal and air temperature predictions from the model at various locations were compared with the rig thermocouple measurements. Wherever there was a discrepancy between the model predictions and thermocouple readings, a multiplication factor in the Nunner correlation of the local stream was adjusted to obtain an improved match. This process is continued until an acceptable match (within ±5 K at steady state and ±15 K at transients) is obtained at all thermocouple locations. Typical temperature matching at thermocouple location 1 is shown in Figure 17. The Nunner Correlation multiplication factors in the matched model were between 0.8 and 1.15, as shown in Table 2, indicating that the Nunner correlation is a good choice for modelling such flows when the CFD-derived 2D flow network is available. When the same FEM model is used to verify the predictions for other test cycles (with different mass flow rates), it was found to be accurate without needing any adjustments in the boundary condition expressions.

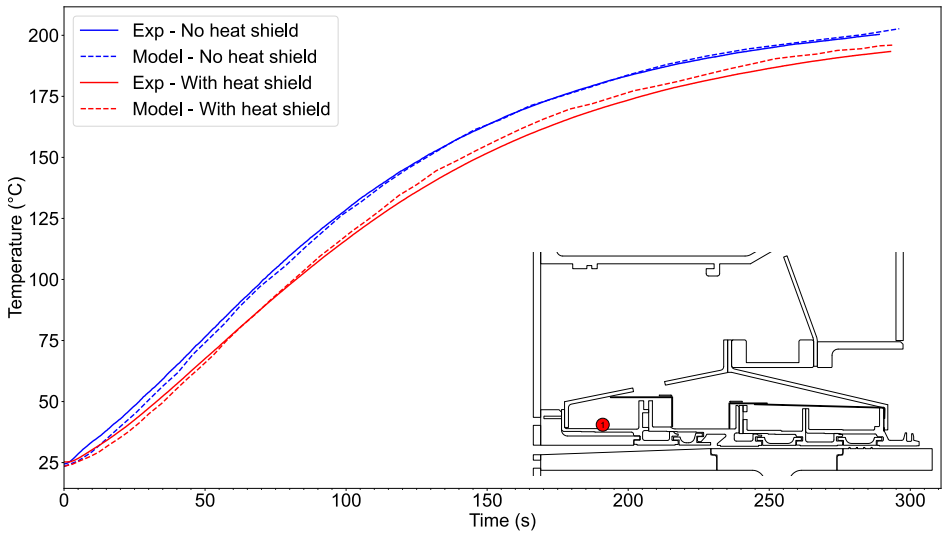

Figure 17. Example at location 1, showing good matching between thermal model and experimental temperature responses.

Table 2. Nunner correlation multiplication factors at five thermocouple locations.

Location	Nunner Multiplier
1	1.1
2	1.15
3	0.8
5	0.85
12	0.9

The metal temperature contours predicted by the FEM for the two cases are shown in Figure 18. The rear part of the inner casing in the heat shielded case is around 25 K cooler than the non-heat shielded case. Showing the rear heat shield performed well in insulating the casing. The insulation effectiveness of the front heat shield was not as effective due to hot ingestion of the offtake flow into the R1 sub-region, caused by an unsealed gap between the heat shield end and the front support cone. In this region, the inner casing in the heat-shielded case was only 5 K cooler than the non-heat-shielded case at stabilized maximum flow condition.

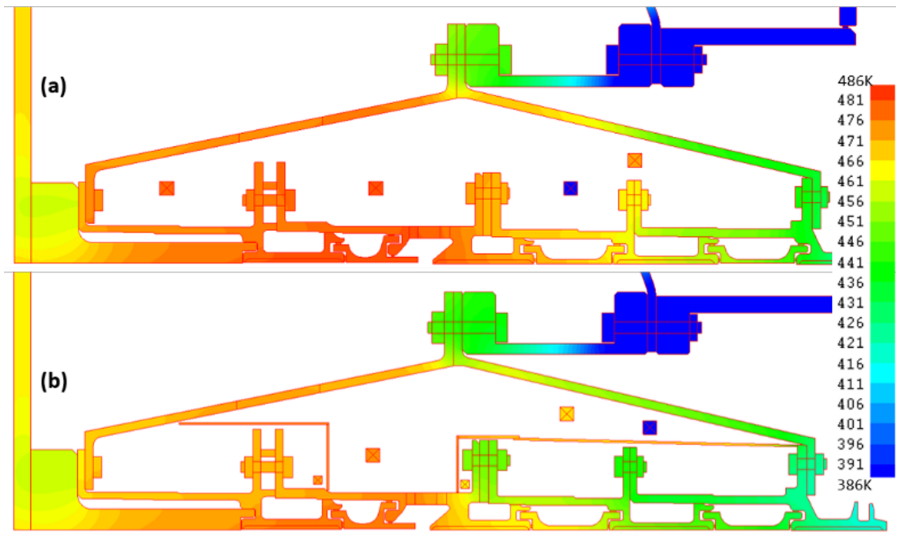

Figure 18. Metal temperature predicted by the FEM models: (**a**) non-heat-shielded case and (**b**) heat-shielded case at stabilized maximum flow condition.

3.7. HTC Comparison

The matched thermal models enable heat transfer coefficients on each surface to be determined; spot points at the twelve thermocouple locations are given in Figure 19.

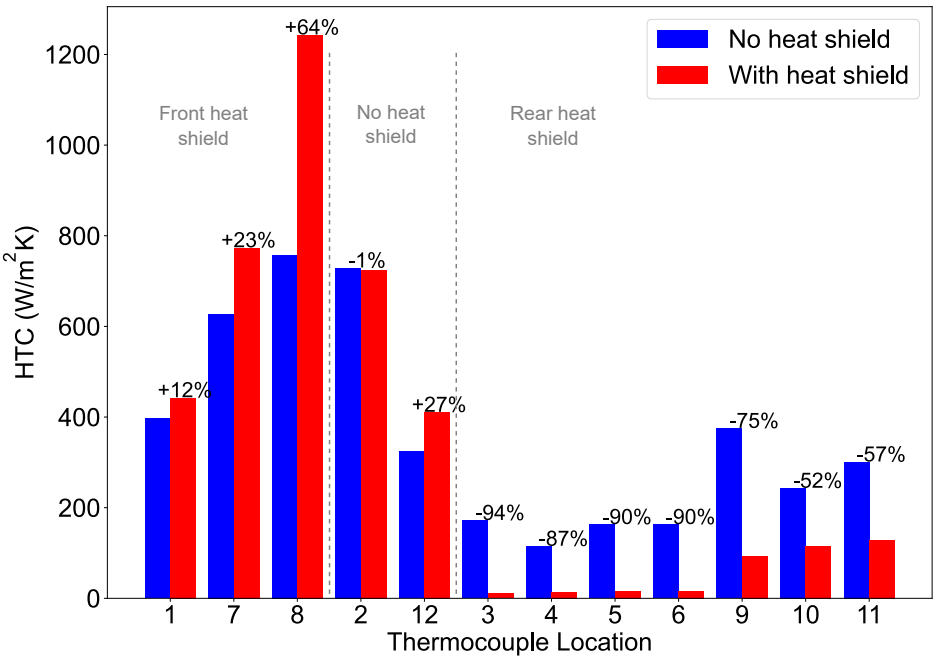

Figure 19. Casing heat transfer coefficients, without and with heat shields fitted.

The locations under the rear heat shield, 3–6 and 9–11, show a significant reduction in heat transfer after the heat shield has been fitted. This shows the rear heat shield is proving effective at reducing the heat transfer to the rear of the casing.

Underneath the front shield at locations 1, 7 and 8, the HTC was found to have increased, rather than decreased as was expected. This is due to leakage flows causing locally higher velocity and hence HTC underneath the heat shield. A further CFD simulation was conducted to include a leakage gap between the front heat shield and support cone. The local high velocity region, causing high HTC, is shown in Figure 20. The leakage flow still has a reduced mass flow and hence a lower enthalpy than the main offtake flow, so the heat flux into the casing is still reduced with the heat shield fitted. This confirms the importance of heat shields being fully sealed against leakage in order to maximise their effectiveness.

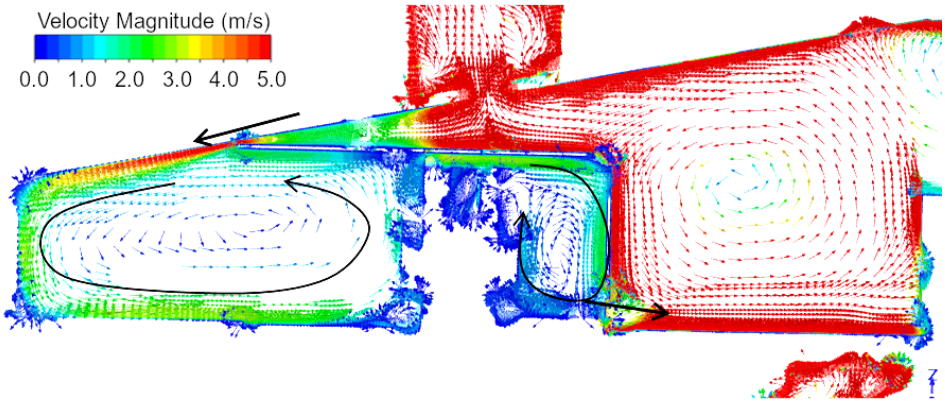

Figure 20. CFD simulation showing local high velocity underneath front heat shield due to leakage flow.

In order to determine the reliability of HTC values predicted by CFD alone, HTC from the matched FEM model is compared with the HTC from the CFD, calculated using Reynolds analogy (Equation (5)). Table 3 shows the comparison for the non-heat shielded case. The CFD predictions were within 11% of the SC03 predictions. Showing that the CFD performed well in predicting the HTC for this complex cavity flow case.

$$h = \frac{\tau_w c_p}{|V| Pr^{0.4}} \tag{5}$$

Table 3. HTC predictions from Reynolds analogy compared to matched thermal model without heat shields.

Location	HTC (W/m^{2}K)		Difference
	Thermal Model	Reynolds Analogy	
1	397	375	−5.5%
2	729	783	+7.4%
3	172	153	−11.0%
5	163	162	−0.1%
12	324	291	−10.2%

The numerical investigation has validated the use of a combination of CFD and FEM to effectively model the complicated flows in offtake cavities.

4. Conclusions

This investigation used a combination of experimental measurements and numerical methods to determine the effectiveness of heat shields in a compressor casing. Measurements were performed on a full-size compressor casing at engine realistic conditions, with back-to-back experiments with and without heat shields fitted. The experimental data gave temperature responses on the casing at several locations, which were used for matching a thermal model.

A numerical investigation was also performed using a combination of CFD and thermal models. The CFD solutions provided a description of the flowfield in the cavity, which was used when setting up the thermal model. The thermal model was then matched to the experimental data, with a good match occurring at all thermocouple locations. This allowed the HTC on the casing to be calculated and the effect of the heat shields on the HTC to be determined.

It was found that the heat shields give an increase in the casing thermal time constant at both the front and rear locations. The rear heat shield was shown to be very effective by significantly reducing the HTC on the rear casing. The front heat shield was effective in reducing the enthalpy of the flow close to the front casing, but this was partially offset by the increase in HTC caused by local high velocities from leaks under the heat shield.

It was also found that the HTC values predicted by the CFD in the offtake cavity agreed well, within 11% of the matched values from the thermal model. This gives confidence in the use of CFD for predictions of compressor casing cavity flows.

The investigation has shown that heat shields can be effective in increasing the thermal time constant of a gas turbine compressor casing. It has also been shown that heat shields must be fully sealed to avoid leaks, as leakage flows can significantly degrade the heat shield's effectiveness.

Author Contributions: Conceptualization, M.B., L.L.; Methodology, L.L., A.P., V.G., C.B.; Validation, A.P., L.L.,V.G., and C.B.; Formal Analysis, A.P., V.G., L.L.; Investigation, A.P., V.G., C.B., L.L.; Writing—Original Draft Preparation, A.P., V.G.; Writing—Review and Editing, A.P.; Supervision, C.B., M.B.; Funding Acquisition, M.B. All authors have read and agreed to the published version of the manuscript.

Funding: This work was supported by the Aerospace Technology Institute UK, in partnership with Rolls-Royce PLC. The financial support and permission for the publication are gratefully acknowledged.

Data Availability Statement: The original contributions presented in this study are included in the article. Further inquiries can be directed to the corresponding author.

Conflicts of Interest: Authors Vinod Gopalkrishna, Christopher Barnes, and Marko Bacic were employed by the company Rolls-Royce. The remaining authors declare that the research was conducted in the absence of any commercial or financial relationships that could be construed as a potential conflict of interest.

Nomenclature

a	Heat transfer source strength
b	Intrinsic time constant
c_p	Specific heat capacity
A	Area for convective heat transfer
M	Mass of solid
D_h	Hydraulic diameter
h	Heat transfer coefficient
k	Thermal conducivity
$\dot{m}$	Mass flow rate
Nu	Nusselt Number $\frac{hD_h}{k}$
Pr	Prandtl Number
Re	Reynolds Number $\frac{\rho V D_h}{\mu}$
T_0	Initial temperature
T_M	Metal temperature
T_{in}	Driving air temperature
V	Flow velocity
λ	Darcy friction factor (rough duct)
λ_0	Darcy friction factor (smooth duct)
μ	Dynamic viscosity
ρ	Density
τ	Thermal time constant
τ_w	Wall shear stress
CFD	Computational Fluid Dynamics
FEM	Finite Element Model
HTC	Heat Transfer Coefficient
THTF	Transient Heat Transfer Facility
HPC	High Pressure Compressor

References

1. Kiss, A.; Spakovszky, Z. Effects of transient heat transfer on compressor stability. *J. Turbomach.* **2018**, *140*, 121003. [CrossRef]
2. Crawford, R.; Burwell, A. Quantitative evaluation of transient heat transfer on axial flow compressor stability. In Proceedings of the 21st Joint Propulsion Conference, Monterey, CA, USA, 8–11 July 1985; p. 1352.
3. Malavade, P.; Babu, S.G.; Frosini, L.; Marchetti, S. Design of Heat Shield for Compressor Case of Industrial Gas Turbine to Meet Clearance Requirement. In Proceedings of the Turbo Expo: Power for Land, Sea, and Air, Online, 21–25 September 2020; American Society of Mechanical Engineers: New York, NY, USA, 2020; Volume 84225.

4. Riahi, A.; Borns, F.G. Gas turbine combustor heat shield impingement cooling baffle. In Proceedings of the Turbo Expo: Power for Land, Sea, and Air, Vienna, Austria, 14–17 June 2004; Volume 41685, pp. 113–123.
5. Pilkington, A.; Gopalkrishna, V.; Barnes, C.; Lewis, L.; Bacic, M. An experimental and numerical investigation into compressor casing heat shield effectiveness. In Proceedings of the 16th European Conference on Turbomachinery Fluid dynamics and Thermodynamics, Hannover, Germany, 24–28 March 2025.
6. Pilkington, A.; Lewis, L.; Bacic, M.; Dann, A. Experimental measurement and characterisation of the effect of offtake flow on the time constants of a compressor casing. In Proceedings of the ETC14 (2021) European Turbomachinery Conference, Online, 12–16 April 2021.
7. van Paridon, A.; Dann, A.; Ireland, P.; Bacic, M. Design and development of a full-scale generic transient heat transfer facility (THTF) for air system validation. In Proceedings of the Turbo Expo: Power for Land, Sea, and Air, Montreal, QC, Canada, 15–19 June 2015; American Society of Mechanical Engineers: New York, NY, USA, 2015; Volume 56727.
8. Dann, A.; Dhopade, P.; Bacic, M.; Ireland, P.; Lewis, L. Experimental and numerical investigation of annular casing impingement arrays for faster casing response. *J. Eng. Gas Turbines Power* **2017**, *139*, 092603. [CrossRef]
9. Nunner, W. *Heat Transfer and Pressure Drop in Rough Tubes*; Atomic Energy Research Establishment: Harwell, UK, 1958.

https://doi.org/10.3390/ijtpp11010009